PCP
PLANT & CELL PHYSIOLOGY

Loss of Chloroplast GNAT Acetyltransferases Results in Distinct Metabolic Phenotypes in *Arabidopsis*

Aiste Ivanauskaite[1], Marjaana Rantala[1], Laura Laihonen[1], Minna M. Konert[1], Naike Schwenner[2], Jens S. Mühlenbeck[2], Iris Finkemeier[2] and Paula Mulo[1,*]

[1]Molecular Plant Biology, Department of Life Technologies, University of Turku, Turku, Finland
[2]Plant Physiology, Institute of Plant Biology and Biotechnology, University of Muenster, Muenster, Germany

*Corresponding author: E-mail, pmulo@utu.fi
(Received 9 December 2022; Accepted 16 March 2023)

Acetylation is one of the most common chemical modifications found on a variety of molecules ranging from metabolites to proteins. Although numerous chloroplast proteins have been shown to be acetylated, the role of acetylation in the regulation of chloroplast functions has remained mainly enigmatic. The chloroplast acetylation machinery in *Arabidopsis thaliana* consists of eight General control non-repressible 5 (GCN5)-related *N*-acetyltransferase (GNAT)–family enzymes that catalyze both N-terminal and lysine acetylation of proteins. Additionally, two plastid GNATs have also been reported to be involved in the biosynthesis of melatonin. Here, we have characterized six plastid GNATs (GNAT1, GNAT2, GNAT4, GNAT6, GNAT7 and GNAT10) using a reverse genetics approach with an emphasis on the metabolomes and photosynthesis of the knock-out plants. Our results reveal the impact of GNAT enzymes on the accumulation of chloroplast-related compounds, such as oxylipins and ascorbate, and the GNAT enzymes also affect the accumulation of amino acids and their derivatives. Specifically, the amount of acetylated arginine and proline was significantly decreased in the *gnat2* and *gnat7* mutants, respectively, as compared to the wild-type Col-0 plants. Additionally, our results show that the loss of the GNAT enzymes results in increased accumulation of Rubisco and Rubisco activase (RCA) at the thylakoids. Nevertheless, the reallocation of Rubisco and RCA did not have consequent effects on carbon assimilation under the studied conditions. Taken together, our results show that chloroplast GNATs affect diverse aspects of plant metabolism and pave way for future research into the role of protein acetylation.

Keywords: Acetylation ● Acetyltransferase ● *Arabidopsis* ● Metabolome ● Photosynthesis ● Rubisco

Introduction

Acetylation is one of the most common chemical modifications found on a variety of molecules ranging from metabolites to proteins involved in all aspects of plant growth and responses to the environment (Drazic et al. 2016, Hartl et al. 2017, Linster and Wirtz 2018, Xue et al. 2018, Tan and Reiter 2020). During *N*-acetylation, an acetyl group is attached to a free amino group of a molecule, such as the N-terminus (NAT) or an internal lysine residue (KAT) of a protein. While acetylation can in certain conditions occur spontaneously, acetylation is mostly catalyzed by acetyltransferase enzymes that use acetyl coenzyme A as a substrate. In recent years, marked progress has been made in understanding the acetylation machinery in different subcellular compartments, with most information being available on nuclear and cytosolic acetyltransferases (Linster and Wirtz 2018, Aksnes et al. 2019). Although a significant amount of acetylation reactions takes place in the chloroplast, the organelle responsible for photosynthesis and a major hub of biosynthesis pathways, only limited information is available about the regulation of acetylation and its impact on chloroplast functions (Finkemeier et al. 2011, Wu et al. 2011, Bienvenut et al. 2012, Hartl et al. 2017, Xue et al. 2018).

The chloroplast acetylation machinery in the model plant *Arabidopsis thaliana* consists of eight General control non-repressible 5 (GCN5)-related *N*-acetyltransferase (GNAT)–family enzymes that are able to catalyze both N-terminal and lysine acetylation (NAT and KAT of proteins (Dinh et al. 2015, Koskela et al. 2018b, Bienvenut et al. 2020). Based on phylogenetic analysis, chloroplast-localized GNAT1, GNAT2 and GNAT3 proteins cluster together and form a subtype 1 of GNAT enzymes, while GNAT4–GNAT7 together with GNAT10 form a distinct subtype 2 (Bienvenut et al. 2020). All chloroplast GNAT enzymes consist of six or seven β-sheets and four α-helices, which are arranged as four conserved domains. Domain A is involved in the acetyl–CoA (Ac–CoA) interaction, domain B is involved in substrate binding and domains C and D have been implicated in the determination of protein stability (Ud-Din et al. 2016). All subtype 1 enzymes and GNAT4, GNAT7 and GNAT10 contain a secondary Ac–CoA binding motif in addition to the main Ac–CoA binding site, which is located at the N-terminus of the α3-helix (Bienvenut et al. 2020). Although all

Plant Cell Physiol. 64(5): 549–563 (2023) doi:https://doi.org/10.1093/pcp/pcad017, Advance Access publication on 17 March 2023, available online at https://academic.oup.com/pcp

chloroplast *GNAT* genes are mainly expressed in green tissues, it is worth noting that the *GNAT6* gene is also expressed in roots (Bienvenut et al. 2020).

The dual NAT/KAT activity sets the plastid GNATs apart from most of the previously characterized GNAT enzymes that predominantly catalyze only one type of acetylation (Liszczak et al. 2011, Magin et al. 2016, Aksnes et al. 2019). The plastid GNATs exhibit relaxed NAT and distinct KAT specificities with some common preferences, suggesting that this unique family of GNATs could share at least some acetylation targets. Nevertheless, the plastid GNAT enzymes also possess distinct substrate specificities in terms of acetylation sites, and the catalytic activities of the GNATs (both for NAT and KAT) differ significantly from each other (Bienvenut et al. 2020). Therefore, the GNAT enzymes appear to play partly redundant and partly specific roles in determining the acetylation profile of the chloroplast proteins in planta.

From the roughly 1,000 N-terminally and 1,000 Lys-acetylated proteins identified in *Arabidopsis* leaf samples, around 30% and 43%, respectively, are predicted to localize in the chloroplast (Hartl et al. 2017, Bienvenut et al. 2020). The functional annotation analysis of Lys-acetylated proteins reveals that photosynthetic proteins are one of the most over-represented groups together with proteins involved in other plastid-related processes, such as tetrapyrrole biosynthesis and redox regulation (Hartl et al. 2017). Several reports have also shown that changes in acetylation affect the activity and/or stability of proteins involved in photosynthesis, namely Rubisco, Rubisco activase (RCA) and ATP synthase, further confirming that acetylation is important for photosynthesis (Finkemeier et al. 2011, Hoshiyasu et al. 2013, Gao et al. 2016, Hartl et al. 2017).

Our work on GNAT2 (NUCLEAR SHUTTLE INTERACTING, NSI or Serotonin N-Acetyltransferase 1, SNAT1), one of the first characterized plastid GNATs, further cements the role of acetyltransferases in photosynthesis. We have shown that GNAT2 is required to balance the excitation energy distribution between the photosystems via state transitions, thus enabling efficient photosynthesis and plant growth under fluctuating light conditions (Koskela et al. 2018b, 2020). The loss of GNAT2 results in decreased N-terminal and Lys-acetylation of several chloroplast proteins that could affect state transitions either by impairing the association of the light-harvesting complex II (LHCII) to photosystem I (PSI) or indirectly by altering the thylakoid structure and dynamics. However, the mechanism behind the state transition phenotype of the *gnat2* mutant remains unknown.

In addition to protein acetylation, two of the plastid GNATs, GNAT1 (SNAT2) and GNAT2, also have been reported to catalyze the acetylation of serotonin and 5-methoxytryptamine (5-MT) in the last steps of melatonin biosynthesis (Lee et al. 2014, 2019). Despite the relatively similar structure (Bienvenut et al. 2020), GNAT1 and GNAT2 show distinct enzymatic properties both as metabolite and protein acetyltransferases. While GNAT1 is more efficient at serotonin acetylation and is inhibited by 5-MT and melatonin, GNAT2 prefers 5-MT acetylation and is inhibited by 5-MT and serotonin (Lee et al. 2014, 2019). Similarly, GNAT1 and GNAT2 differ in specificity and activity as protein acetyltransferases: they prefer different Lys-acetylation sites, and unlike GNAT2, GNAT1 shows only weak NAT activity (Bienvenut et al. 2020). The fact that the GNAT1 and GNAT2 enzymes are able to acetylate not only proteins but also metabolites raises the question whether some of the remaining plastid GNATs could also have a role in metabolite biosynthesis.

Here, we have characterized six of the plastid GNATs using a reverse genetics approach with metabolic profiling and a special focus on photosynthesis. Our results reveal the impact of GNAT enzymes on the accumulation of various compounds, most interestingly lipids (including oxylipins) and the antioxidant ascorbate. In addition, the GNAT enzymes affect the accumulation of amino acids and their (acetylated) derivatives. Our study also further supports earlier findings showing the role of GNAT2 in the function of photosynthetic light harvesting, as seen by increased phosphorylation of thylakoid proteins and increased non-photochemical quenching (NPQ) in the *gnat2* mutant. Interestingly, knocking out of any of the GNAT enzymes increases the membrane recruitment of Rubisco and RCA, suggesting that changes in global acetylation levels may affect carbon assimilation enzymes. Taken together, our results suggest that the chloroplast GNATs play a multifaceted role in plant metabolism and its regulation.

Results

Acetyltransferase mutants share similar metabolic features

To unravel the physiological roles of the plastid GNAT enzymes, we have taken a reverse genetics approach and characterized homozygous T-DNA insertion lines for *gnat1*–*gnat7* and *gnat10* (**Supplementary Fig. S1**). End-point RT-PCR and/or quantitative RT-PCR analyses of transcript abundance confirmed that the freely available T-DNA lines for *gnat1*, *gnat2*, *gnat4*, *gnat7* and *gnat10* are complete knock-outs, while for *gnat6*, the results obtained with two primer pairs were inconclusive (**Supplementary Fig. S2**, Koskela et al. 2018b). In addition, *gnat3* lines contained wild-type levels of *GNAT3* mRNA, and *gnat5* was found to be an over-expressor, and therefore these lines were excluded from further analysis (**Supplementary Fig. S2**).

To get insight into the function of each GNAT and their possible role as metabolite acetyltransferases, we performed non-targeted metabolic profiling of 3-week-old rosettes of complete *gnat* knock-outs (*gnat1*, *gnat2*, *gnat4*, *gnat7* and *gnat10*) utilizing UHPLC–quadrupole time-of-flight–MS. The full list of detected significantly changed metabolites (111 compounds) is presented in **Supplementary Dataset S1 and Fig. S3**, while the selected metabolites of interest are also

Table 1 Shared features in the metabolome of the *gnat* mutants

		Fold-changes with *q*-value of < 0.1 (<0.01 in bold)				
Curated ID	Compound class	*gnat1* vs. Col-0	*gnat2* vs. Col-0	*gnat4* vs. Col-0	*gnat7* vs. Col-0	*gnat10* vs. Col-0
Ascorbic acid	Vitamin		0.27	0.18	0.15	0.19
OxoOTrE (isomer 1)	Oxylipin			0.68	**0.66**	**0.69**
FA 13:3+1O	Oxylipin		0.38	0.36	0.34	0.37
HpOTrE (isomer 3)	Oxylipin		0.60	0.59	0.56	0.56
FA 18:4+2O (isomer 1)	Oxylipin		0.51	0.60	0.58	0.54
EpKODE (isomer 1)	Oxylipin			0.74	0.76	0.74
HpOTrE (isomer 2)	Oxylipin		0.62	0.67	0.61	0.56
EpKODE (isomer 2)	Oxylipin		0.63		0.63	0.61
dnOPDA (isomer 1)	Octadecanoid		0.60	0.69	0.62	0.57
Serine	Amino acid	**1.69**	1.42	**1.53**	1.35	**1.55**
MGDG (18:3/16:3) (isomer 1)	Glycosyldiradyl-glycerol		1.81	**2.08**	**1.96**	**2.12**
MGDG (18:3/16:3) (isomer 2)	Glycosyldiradyl-glycerol		1.35	1.42		**1.53**
MGDG (18:3/18:3)	Glycosyldiradyl-glycerol			1.34	1.29	**1.56**
DG (18:3/18:3) (dilinolenin)	Diacylglycerol		**1.31**	1.31		1.33
LPG (18:3)	Lysophosphatidylglycerol		**1.47**	1.38	1.39	**1.61**

FCs of the selected metabolites that behave similarly in at least four *gnat* lines ($n = 5$). The FDR-corrected *P*-value (*q*-value) was used to assess the significance of the observed changes using 0.1 as the cutoff. FC values with $q > 0.1$ were omitted and are indicated with a dash. Abbreviations: OxoOTrE, oxo-octadecatrienoic acid, EpKODE, epoxy-keto-octadecadienoic acid.

presented in **Tables 1** and **2**. The lack of specific GNAT enzymes resulted in significant changes in the metabolome, but the extent varied depending on the affected enzyme (**Supplementary Fig. S3, Dataset S1**). Depletion of GNAT1 affected the accumulation of four distinct metabolites, while the inactivation of GNAT10 resulted in changes in the content of 89 metabolites (**Supplementary Dataset S1**). The remaining mutants, *gnat2*, *gnat4* and *gnat7*, showed significant changes in the amount of 28, 46 and 38 metabolites compared to Col-0, respectively (**Supplementary Dataset S1**). Although most of the significantly changed metabolites showed increased accumulation compared to Col-0, all mutant lines (except *gnat1*) also contained some metabolites with decreased levels (**Supplementary Fig. S3, Dataset S1**). The most striking change was observed in two acetylated metabolites: the level of N_{α}-acetyl-L-arginine was markedly decreased in *gnat2* [fold change (FC) 0.108], while the content of *N*-acetylproline was severely reduced in *gnat7* (FC 0.015) (**Supplementary Dataset S1**).

Intriguingly, defects in almost any of the GNAT enzymes resulted in some shared features in the metabolome. For instance, all *gnat* mutants (with the exception of *gnat1*) showed reduced levels of the antioxidant ascorbate, plastid lipid-derived jasmonic acid (JA) biosynthesis intermediate dinor-12-oxophytodienoic acid (dnOPDA) (Weber et al. 1997, Schaller and Stintzi 2009) and various oxylipins, such as hydroperoxyl-octadecatrienoic acid (HpOTre; **Table 1**, **Supplementary Dataset S1**). Concomitantly, an increase in the level of the amino acid serine was detected in all mutant lines, and the content of some lipids, i.e. monogalactosyldiacylglycerol (MGDG), diacylglycerol (DG) and lysophosphatidylglycerol (LPG 18:3) (**Table 1**, **Supplementary Dataset S1**), was increased in most *gnat* mutants as compared to Col-0. Additionally, many other metabolites of unknown function, as well carnitine and proline, showed similar trends in most *gnat* mutants, although the changes were not statistically significant (**Supplementary Fig. S3, Dataset S1**).

The *gnat* mutants possess unique metabolic profiles

Among the mutant lines, the inactivation of GNAT10 resulted in the most significant change in the metabolome. In addition to changes in the metabolites affected in most *gnat* mutants, *gnat10* showed a slight, but statistically significant, increase in the levels of free amino acids, various di- and tripeptides and several nucleosides and nucleobases (**Table 2**, **Supplementary Dataset S1**). The content of the lipid linoleic acid was considerably increased (FC 1.66) as compared to Col-0. Several stress-related compounds were also increased in *gnat10*. Specifically, the level of tryptophan-derived indole-3-carboxylic acid and methoxyindole-3-carbaldehyde (Böttcher et al. 2014) was increased ca. 1.5-fold compared to Col-0, while the level of the glucosinolate glucohirsutin together with the isothiocyanate formed upon its cleavage, hirsutin, was slightly less affected (**Table 2**, **Supplementary Dataset S1**). Similarly, the content of hirsutin was increased in *gnat4* and *gnat7* mutants.

Most of the metabolites with changed accumulation in the *gnat4* mutant were shared with one or more *gnat* mutant lines (**Table 1**, **Supplementary Dataset S1**). However, the lysophospholipid lysophosphatidylethanolamine (LPE 16:0) was somewhat decreased, and the nucleobase methylguanine increased specifically in *gnat4* (**Table 2**, **Supplementary Dataset S1**). The *gnat7* mutant, on the other hand, showed specific changes in several metabolites of potential interest. The most noteworthy feature of the *gnat7* metabolome was the strong decrease in the level of *N*-acetylproline as compared to Col-0. In addition, the level of the phenylpropanoid sinapine, the glucosinolate-derived isothiocyanate sulforaphane and the auxin-conjugate indole-3-acetyl-L-alanine

Table 2 Unique metabolic features of specific *gnat* mutant lines

Mutant line/curated ID	Compound class	FC, *q*-value < 0.1 (<0.01 in bold)
gnat2		
N_{α}-acetyl-L-arginine	Amino acid	**0.11**
Proline	Amino acid	0.55
gnat4		
LPE (16:0)	Lysophosphatidyl-ethanolamine	0.71
Methylguanine	Nucleobase	1.27
gnat7		
N-acetylproline	Amino acid	**0.01**
Sinapine	Betaine	2.19
Indole-3-acetyl-L-alanine	Indole	**1.53**
Sulforaphane	Isothiocyanate	1.55
gnat10		
Carnitine (also in *gnat7*)	Amino acid	0.68
Citrulline (also in *gnat2*)	Amino acid	1.28
Tyrosine	Amino acid	1.32
Asparagine	Amino acid	1.32
Threonine	Amino acid	1.29
Lysine	Amino acid	1.39
Pro-Arg	Dipeptide	1.25
Lys-Ser	Dipeptide	1.25
Ala-His	Dipeptide	1.36
Gln-Asn	Dipeptide	1.40
Pro-Gly	Dipeptide	1.34
Phe-Ile-Lys	Tripeptide	1.79
Ala-Gly-Lys	Tripeptide	**1.31**
2-*O*-Methyladenosine (also in *gnat4*)	Nucleoside	**1.67**
Guanosine	Nucleoside	1.48
Adenine	Nucleobase	1.25
Adenosine	Nucleoside	1.27
Uridine	Nucleoside	1.31
Deoxyadenosine	Nucleoside	1.41
Methylthioadenosine	Nucleoside	1.23
Linoleic acid (18:2)	PUFA	**1.66**
Indole-3-carboxylic acid	Indole	**1.50**
Methoxyindole-3-carbaldehyde (isomer 1)	Indole	**1.56**
Hirsutin (also in *gnat4* and *gnat7*)	Sulfoxide isothiocyanate	1.30
Glucohirsutin	Glucosinolate	1.29

FCs of the selected metabolites that show changed levels specific to one *gnat* mutant line as compared to Col-0 ($n = 5$). The FDR-corrected *P*-value (*q*-value) was used to assess the significance of the observed changes using 0.1 as the cutoff.

(Ludwig-Müller 2011) was increased upon GNAT7 inactivation (**Table 2**, **Supplementary Dataset S1**). The inactivation of GNAT1 affected only four metabolites that showed changes in other *gnat* lines as well (**Table 1**, **Supplementary Dataset S1**). However, among the mutant lines, the increase in the content of serine was the highest (FC 1.69) and most significant in the *gnat1* line as compared to Col-0 (**Table 2**, **Supplementary Dataset S1**).

In the *gnat2* metabolome, the most striking change was the strong decrease in N_{α}-acetyl-L-arginine (FC 0.11) (**Table 2**). It is worth noting that the amount of free proline was also markedly decreased in *gnat2* (FC 0.55), although a similar, yet statistically insignificant, trend was observed in all the other *gnat* lines as well. Because GNAT2 has been shown to catalyze acetylation of serotonin in the biosynthetic pathway of melatonin (Lee et al. 2014), and the loss of GNAT2 resulted in marked changes in the photosynthetic properties of the plant (Koskela et al. 2018a, 2020), we aimed to quantify the melatonin level in the *gnat2* mutant. Since melatonin was not detected in the initial untargeted metabolic profiling, we analyzed the melatonin content of the *gnat2* line using an alternative ultra-performance liquid chromatography (UPLC)–MS approach. In agreement with previous results (Lee and Back 2018), the melatonin content of *gnat2* rosettes grown under standard conditions was not decreased but rather slightly higher than that in Col-0 (**Supplementary Fig. S4**), indicating that GNAT2 is not essential for melatonin production under standard growth conditions.

The lack of GNAT2 affects plant growth and photosynthetic properties

Several metabolites with changed accumulation in the *gnat* mutants (e.g. ascorbate, oxylipins and MGDG) have an important role in photosynthesis. These results together with the previously reported role of GNAT2 in photosynthesis (Koskela et al. 2018a, 2020) and the high prevalence of acetylation among photosynthetic proteins (Finkemeier et al. 2011, Wu et al. 2011, Hartl et al. 2017) prompted us to turn our attention to the growth phenotype and photosynthetic properties of the *gnat* mutants. As the distinct mutants may respond differently under growth-light (GL) conditions, we grew the mutant plants in short-day conditions under three different light intensities of PPFD 100, 130 and 160 μmol m^{-2} s^{-1}. Indeed, *gnat2* showed slightly retarded growth as compared to Col-0 (**Fig. 1**, **Supplementary Fig. S5**). The growth phenotype of *gnat2* was light-dependent, as the growth defect diminished when plants were grown under high-light (HL) intensities (**Fig. 1B**, **Supplementary Fig. S5**, Koskela et al. 2020, Lee and Back 2021). While the chlorophyll (Chl) *a* and *b* content was similar in all mutant lines, the Chl *a* to *b* ratio was lower in *gnat2* when compared to Col-0 as previously reported by Koskela et al. (2018b) (**Supplementary Table S3**). These results emphasize the role of GNAT2 in the growth and development of the plant, while the remaining GNATs did not impact growth, at least under the indicated growth conditions.

To assess whether the lack of GNATs results in changes in photosynthetic function, we performed light curve measurements of the *gnat* lines compared to Col-0 using DUAL-PAM. As previously reported by Koskela et al. (2018b), our results showed that the *gnat2* mutant showed a marked increase in the quantum yield of nonregulated energy dissipation [Y(NO)] at light intensities below GL, while the photosynthetic properties of other *gnat* mutants did not differ from those of Col-0 (**Table 3**, **Supplementary Dataset S2**). Moreover, *gnat2* plants exhibited slightly higher NPQ than Col-0 in light intensities with a PPFD of >500 μmol m^{-2} s^{-1} (**Table 3**, **Supplementary Dataset S2**), as reported by Koskela et al. (2018b, 2020). Despite the NPQ differences detected in *gnat2*, the accumulation of the PSBS protein and violaxanthin de-epoxidase (VDE), the key players in the induction of NPQ (Jahns and Holzwarth 2012), did not differ between any of the *gnat* mutants and Col-0 (**Supplementary Fig. S6A**). In accordance with this, the HL-induced dynamics of xanthophyll cycle pigments antheraxanthin, zeaxanthin and

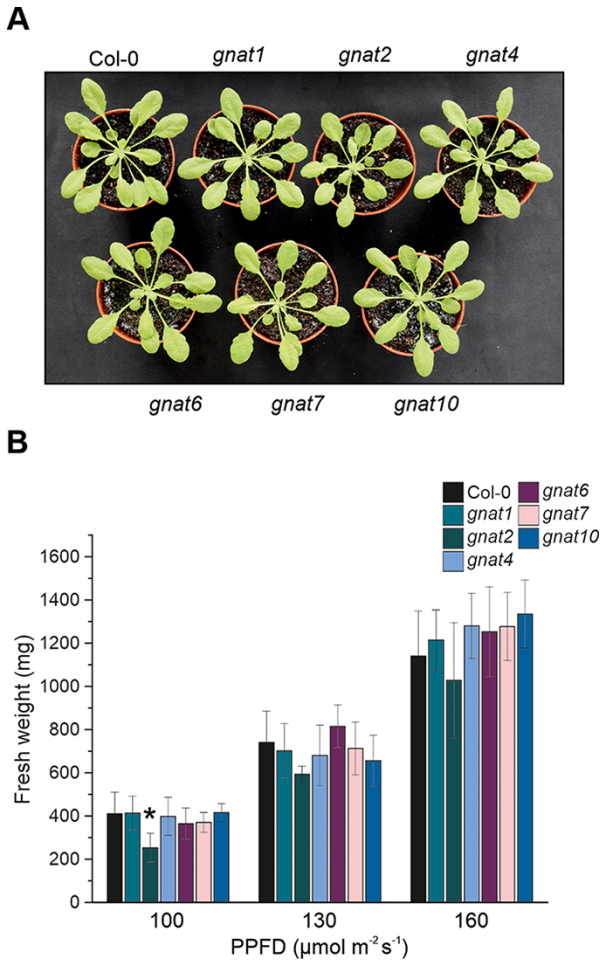

Fig. 1 The growth phenotype of *gnat* mutant lines. (A) 5-week-old *gnat* mutant plants grown at a PPFD of 100 μmol m^{-2} s^{-1} under 8-h light/16 dark cycles at + 23°C and relative humidity 50–55%. (B) Fresh weights of 5-week-old *gnat* plants grown at a PPFD of 100, 130 or 160 μmol m^{-2} s^{-1}. $n = 5–6$. The statistically significant ($P < 0.05$) difference (compared to Col-0) is indicated with an asterisk.

violaxanthin were also unchanged in *gnat2* (**Supplementary Fig. S6B**). The xanthophyll cycle was also unaffected in *gnat1* and *gnat10* mutants. These two lines were selected for pigment analysis based on similarity to GNAT2 and marked changes in the metabolome, respectively (**Supplementary Fig. S6B**). To further dissect the NPQ dynamics in the *gnat* mutants, we performed electrochromic shift (ECS) measurements that revealed no differences in the magnitude or partitioning of the proton motive force (*pmf*), which is required for NPQ induction, or in ATP synthase conductivity (**Supplementary Dataset S3**).

The GNAT enzymes affect thylakoid recruitment of Rubisco and RCA

It was previously reported that the loss of GNAT2 resulted in drastic reorganization of thylakoid protein complexes (Koskela et al. 2018b). Specifically, the accumulation of the 'state transition complex', i.e. PSI–LHCII, was not detectable in the *gnat2* mutants. This defect was directly reflected in photosynthetic regulation, as state transitions were severely dysfunctional (Koskela et al. 2018b). To study the impact of other GNAT enzymes on the organization of thylakoid protein complexes, we subjected the *gnat* mutants to blue native polyacrylamide gel electrophoresis (BN-PAGE; **Fig. 2A**, **Supplementary Fig. S7**) (Rantala et al. 2018). Indeed, upon solubilizing the non-appressed regions of the thylakoid membrane with the mild detergent digitonin followed by the BN-PAGE analysis, no accumulation of the PSI–LHCII complex was detected in *gnat2*, while no such defect was recorded in other *gnat* mutants (**Fig. 2A**). Solubilization of whole thylakoids with β-dodecyl maltoside showed almost identical organization and accumulation of the thylakoid protein complexes participating in photosynthetic electron transfer in all plant lines (**Supplementary Fig. S7**). Moreover, no differences were detected between the plant lines, when the accumulation of thylakoid proteins was studied by SDS-PAGE and immunoblotting using antibodies against protein subunits representing PSII, LHCII, Cyt b_6f and PSI (**Fig. 2B**, **Supplementary Fig. S8**). The amount of ATP synthase subunits ATP-f and ATP-β was slightly decreased in the *gnat4 and gnat6* mutants, respectively (**Fig. 2B Supplementary Fig. S8**).

Intriguingly, one band appeared more intense in all *gnat* lines when the BN gels were stained with Coomassie (**Fig. 2A**, **Supplementary Fig. S7**). To identify the protein complex showing increased accumulation, the subunits of each protein complex on BN were resolved on a denaturing SDS-PAGE gel and the gel was stained with SYPRO protein stain. The protein complex showing higher accumulation in the *gnat* lines was identified as Rubisco (**Supplementary Fig. S7**) based on Aro et al. (2005). As Rubisco is mainly present in a soluble form in chloroplast stroma, we further measured the amount of Rubisco both in thylakoid and in total protein samples. Immunoblot analysis confirmed that *gnat* thylakoid samples contain around 1.5–2 times more of the large subunit of Rubisco (RbcL) than Col-0 samples, while the level of RbcL was not changed in the total protein extract (**Fig. 2C**, **Supplementary Fig. S7**). Thus, the loss of the GNAT enzymes did not have an impact on the overall accumulation but rather on the recruitment of Rubisco to the thylakoids. An even greater increase in the thylakoid fraction was observed for RCA (**Fig. 2C**, **Supplementary Fig. S7**). To see if other stromal proteins accumulate to a higher degree in the thylakoid samples of the *gnat* mutants, we also compared the amount of ferredoxin:NADP(H) oxidoreductase-like (FNRL) and leaf-type ferredoxin-NADP(H) oxidoreductase (FNR) in thylakoid and total protein samples. FNRL is a fully soluble stromal protein (Koskela et al. 2018b), while FNR is found both in the stroma and associated with the thylakoids depending on the chloroplast redox state (Lintala et al. 2007, Benz et al. 2009). However, no significant increase in FNRL or FNR was observed in the thylakoid samples (**Fig. 2**).

Table 3 Photosynthetic parameters obtained from light curve measurements with DUAL-PAM

Line	PPFD (μmol m^{-2} s^{-1})	Y(II)	Y(NO)	NPQ	qP	Y(I)	Y(ND)	Y(NA)
Col-0	50	0.65 ± 0.02	0.28 ± 0.013	0.23 ± 0.025	0.89 ± 0.01	0.71 ± 0.017	0.1 ± 0.048	0.19 ± 0.036
	700	0.08 ± 0.018	0.32 ± 0.019	1.88 ± 0.121	0.15 ± 0.026	0.12 ± 0.029	0.8 ± 0.027	0.08 ± 0.003
gnat1	50	0.66 ± 0.029	0.27 ± 0.016	0.23 ± 0.044	0.88 ± 0.026	0.73 ± 0.019	0.06 ± 0.03	0.21 ± 0.023
	700	0.11 ± 0.022	0.3 ± 0.021	2.01 ± 0.135	0.19 ± 0.038	0.15 ± 0.029	0.77 ± 0.039	0.08 ± 0.02
gnat2	50	0.61 ± 0.015	**0.34 ± 0.013**	0.16 ± 0.013	**0.82 ± 0.03**	0.72 ± 0.036	0.04 ± 0.008	0.24 ± 0.036
	700	0.1 ± 0.012	0.29 ± 0.005	2.1 ± 0.053	0.19 ± 0.016	0.16 ± 0.016	0.77 ± 0.031	0.07 ± 0.018
gnat4	50	0.65 ± 0.027	0.28 ± 0.009	0.25 ± 0.053	0.9 ± 0.01	0.71 ± 0.023	0.11 ± 0.054	0.18 ± 0.036
	700	0.08 ± 0.01	0.33 ± 0.011	1.8 ± 0.075	0.14 ± 0.011	0.12 ± 0.019	0.81 ± 0.023	0.07 ± 0.012
gnat6	50	0.69 ± 0.016	0.26 ± 0.013	0.18 ± 0.013	0.9 ± 0.006	0.72 ± 0.006	0.06 ± 0.014	0.22 ± 0.016
	700	0.1 ± 0.007	0.31 ± 0.019	1.87 ± 0.152	0.17 ± 0.014	0.14 ± 0.006	0.79 ± 0.01	0.07 ± 0.014
gnat7	50	0.67 ± 0.034	0.26 ± 0.013	0.26 ± 0.074	0.92 ± 0.019	0.71 ± 0.032	0.09 ± 0.048	0.19 ± 0.049
	700	0.09 ± 0.018	0.31 ± 0.018	1.94 ± 0.124	0.18 ± 0.023	0.14 ± 0.026	0.8 ± 0.034	0.06 ± 0.017
gnat10	50	0.68 ± 0.006	0.27 ± 0.002	0.19 ± 0.032	0.9 ± 0.012	0.7 ± 0.016	0.08 ± 0.034	0.22 ± 0.03
	700	0.09 ± 0.014	0.32 ± 0.016	1.84 ± 0.111	0.17 ± 0.023	0.14 ± 0.014	0.79 ± 0.016	0.07 ± 0.001

Plants grown for 6 weeks at a PPFD of 110 μmol m^{-2} s^{-1} were dark-adapted for 30 min and exposed to 5-min illumination steps at the PPFDs of 50, 75, 100, 125, 150, 250, 500, 700 and 1,000 μmol m^{-2} s^{-1}. Parameters included in the table were calculated after the illumination with PPFDs of 50 and 700 μmol m^{-2} s^{-1}. The measurement was performed on 3–4 plants/line. Abbreviations: Y(II), quantum yield of photosystem II; Y(NO), quantum yield of nonregulated energy dissipation; qP, coefficient of photochemical quenching; Y(I), quantum yield of PSI; Y(ND), non-photochemical quantum yield of PSI, donor side; Y(NA), non-photochemical quantum yield of PSI, acceptor side. Values with a statistically significant ($P < 0.05$) difference (compared to Col-0) are in bold.

To explore the impact of the increased amount of Rubisco and RCA attached to the thylakoids, we next focused on the carbon assimilation efficiency of *gnat1*, *gnat2* and *gnat10* mutants because the catalytic activities (Lee and Back 2018, Lee et al. 2019, Li et al. 2020) and protein acetylation efficiencies (Koskela et al. 2018b, Bienvenut et al. 2020) of these enzymes differ markedly from each other. However, gas exchange measurements revealed no differences in CO_2 assimilation between the mutant lines and Col-0 plants when carbon assimilation was measured in response to different light intensities or CO_2 concentrations (**Supplementary Fig. S9**), indicating that the reallocation of Rubisco and RCA to the thylakoid fraction does not have measurable consequences on the efficiency of carbon fixation in planta.

Loss of GNAT2 has an impact on the phosphorylation of thylakoid proteins, while the PSII repair cycle is not affected

Protein phosphorylation is known to be one of the major regulators of photosynthetic light reactions, and lately, there has been speculation about the interplay of protein phosphorylation and acetylation (Schmidt et al. 2017, Uhrig et al. 2019). To see if the absence of the studied GNATs has an impact on protein phosphorylation, thylakoid proteins of *gnat* mutants were separated using SDS-PAGE and the gel was stained with ProQ Diamond stain, which is specific for phosphorylated proteins. Our results show a significant increase in the phosphorylation of the photosynthetic LHCII proteins and the core subunits of PSII in *gnat2* under standard growth conditions, while no consistent changes were observed in the phosphorylation pattern of the other *gnat* mutants as compared to Col-0 (**Fig. 3A**, **Supplementary Fig. S10**). Interestingly, the increase in protein phosphorylation in *gnat2* was less apparent, when detected using an antibody against phosphorylated threonine (**Supplementary Fig. S10**). Due to the clearly increased phosphorylation of *gnat2* thylakoid proteins, we next studied how the phosphorylation pattern was affected by an HL treatment with a PPFD of 1,000 μmol m^{-2} s^{-1}. Under HL conditions, LHCII of *gnat2* remained hyperphosphorylated, while the phosphorylation of PSII core proteins appeared slightly, yet not statistically significantly, decreased as compared to Col-0 (**Fig. 3A**, **Supplementary Fig. S10**).

Because phosphorylation plays a crucial role in the repair cycle of photodamaged PSII, thus maintaining the function of the photosynthetic machinery in (high) light through light-induced degradation and concomitant biosynthesis of the PSII core protein D1 (Aro et al. 1993), we studied the susceptibility of PSII to photoinhibition (and thereby the efficiency of PSII repair). To that end, we subjected *gnat1*, *gnat2* and *gnat10* leaves to moderate HL (PPFD 600 μmol m^{-2} s^{-1}) followed by recovery at GL (PPFD 130 μmol m^{-2} s^{-1}) while simultaneously monitoring their photosynthetic capacities (F_v/F_m) and D1 protein levels. To reveal the impact on both protein synthesis and degradation, the experiment was done in the absence and in the presence of lincomycin, an inhibitor of chloroplast protein translation. The results show that despite differences in phosphorylation, the PSII capacity and D1 protein content in the mutants did not differ from those of Col-0 (**Fig. 3B, C**). The relatively mild HL treatment induced only a moderate decrease in the quantum yield of PSII (F_v/F_m), as all lines retained 90% of their initial activity at the end of the 2-h HL treatment (**Fig. 3B**). In line with this, D1 protein levels remained unchanged throughout the HL treatment in all lines, indicating no defects in the D1 protein synthesis or in the D1 degradation during the PSII repair cycle (**Fig. 3B**). As expected, the PSII quantum yield showed a more marked decrease in the lincomycin-treated leaves, going to around 60% at the end of the HL treatment (**Fig. 3C**). D1 levels decreased to roughly 80% of the starting point (**Fig. 3C**), reflecting the relatively slower process of protein degradation. A harsher treatment at 1,000 μmol m^{-2}

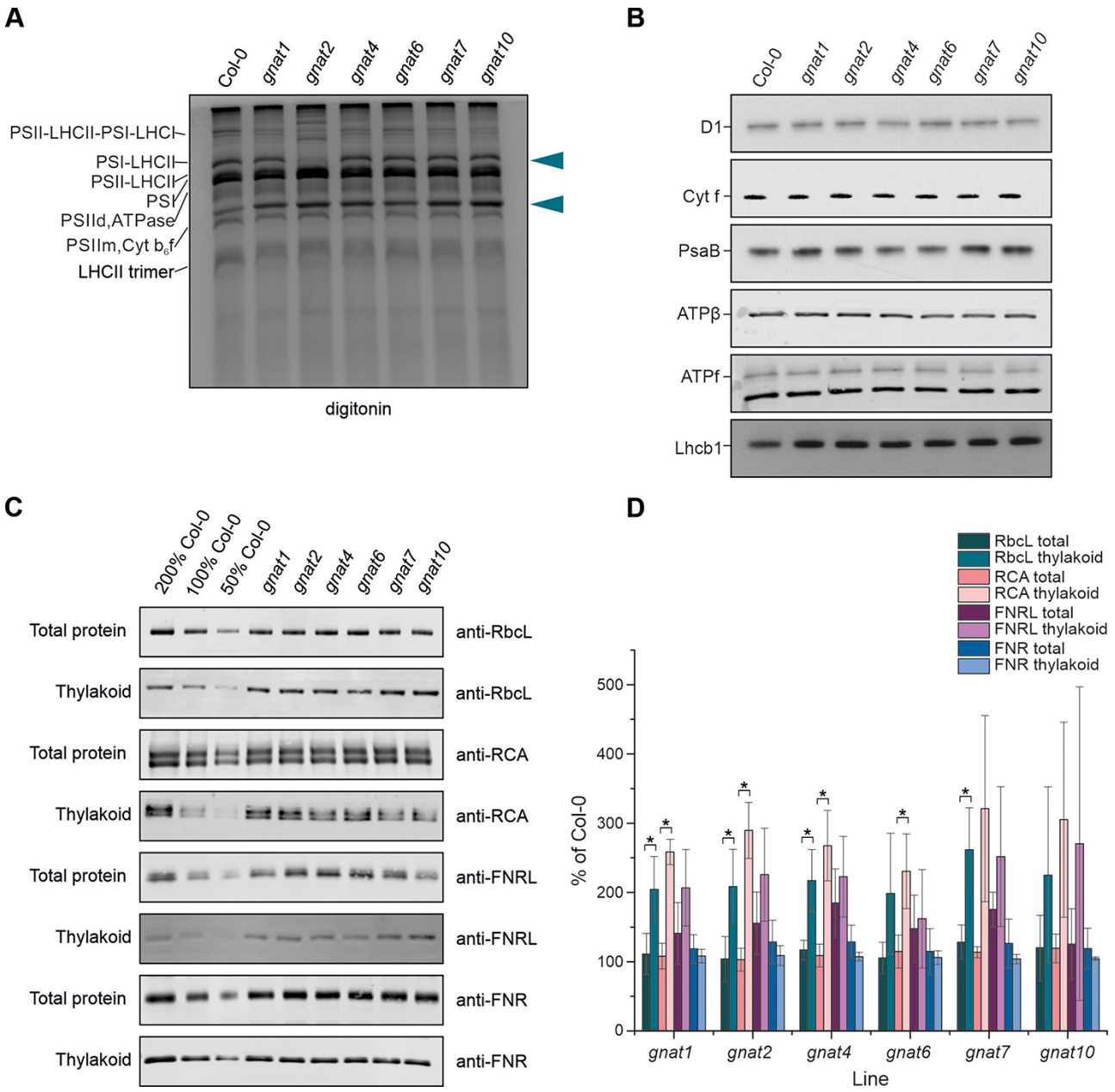

Fig. 2 An analysis of thylakoid protein complexes and selected stromal proteins in the *gnat* mutants. (A) *gnat* mutant thylakoid samples solubilized with digitonin and separated on a BN gel and stained with Coomassie. Bands corresponding to PSI–LHCII and Rubisco are indicated with arrows. A representative gel from three biological replicates is shown. (B) Immunoblot analysis of *gnat* thylakoid proteins using antibodies against D1, cytochrome f (Cyt f), PsaB, ATPβ, ATPf and Lhcb1 proteins. Representative results from three biological replicates are shown. (C) Immunoblot analysis using antibodies against Rubisco L subunit (RbcL), RCA, FNRL and leaf-type FNR (FNR) with total and thylakoid protein samples. Representative immunoblots from three biological replicates are shown. (D) The quantification of immunoblot results used to assess the amount of Rubisco, RCA, FNRL and FNR in total and thylakoid protein samples of *gnat* mutants ($n = 3$). Statistically significant ($P < 0.05$) comparisons are indicated with asterisks.

s^{-1} resulted in a stronger decrease in F_v/F_m values to roughly 35–40% of starting point when protein translation was not blocked and to 5–10% of starting point in leaves treated with lincomycin, but no differences were observed between the lines (**Supplementary Dataset S4**).

Discussion

Acetylation of proteins has been shown to affect a significant amount of chloroplast proteins, likely through the action of eight plastid-localized GNAT acetyltransferase enzymes

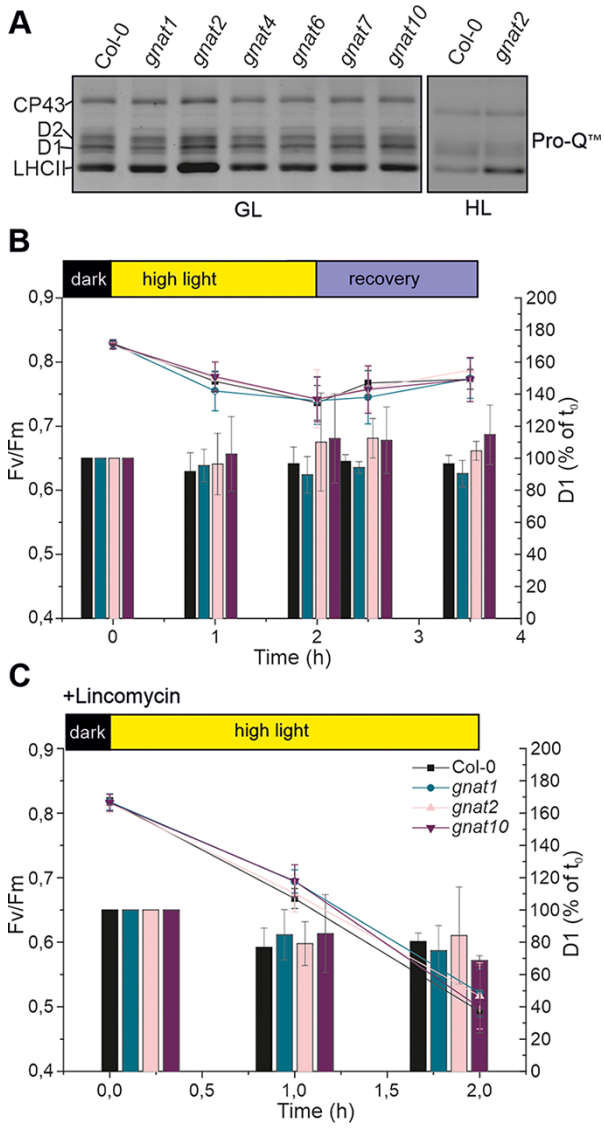

Fig. 3 Thylakoid protein phosphorylation and the abundance of D1 protein under photoinhibitory conditions. (A) Thylakoid phosphoproteins from standard growth conditions (GL) and after a 2-h HL treatment at a PPFD of 1,000 μmol m^{-2} s^{-1} separated on an SDS-PAGE gel and visualized using Pro-Q™ Diamond stain. Representative results from three biological replicates are shown. PSII photoinhibition and D1 turnover monitored in *gnat1*, *gnat2* and *gnat10* samples treated (B) for 2 h at a PPFD of 600 μmol m^{-2} s^{-1} and 1.5-h recovery at GL (130 μmol photons m^{-2} s^{-1}) and (C) for 2 h at 600 μmol photons m^{-2} s^{-1} using lincomycin to inhibit protein translation in the chloroplast. The amount of active PSII was assessed by measuring PSII yield (F_v/F_m, indicated as lines, $n = 5$–6) and D1 protein levels (indicated as bars) compared to the beginning of the treatment (t_0, $n = 3$).

(Bienvenut et al. 2020). Each plastid GNAT enzyme has a unique specificity, indicating that the GNAT enzymes have distinct physiological roles in plant metabolism (Lee et al. 2014, 2019, Dinh et al. 2015, Bienvenut et al. 2020). However, the relaxed N-terminal acetylation activity of GNAT-family enzymes suggests that they are also likely to have some redundancy, thus adding to the robustness of the acetylation machinery in the chloroplast (Bienvenut et al. 2020). In line with this, the loss of GNAT enzymes resulted in various shared features in the plant metabolome and photosynthesis-related processes between the studied mutants. In particular, the decrease in the amount of oxylipins and the increased allocation of the carbon assimilation enzymes Rubisco and RCA to the thylakoid fraction are of potential interest and suggest that acetylation affects key processes of the chloroplast. In addition to the shared features of the *gnat* mutants, some specific differences were also observed pointing to specific roles of the GNAT enzymes in photosynthesis and amino acid metabolism.

Chloroplast acetyltransferases affect the accumulation of oxylipins

Oxylipins are a group of oxidized lipid derivatives produced either enzymatically and/or chemically via hydroperoxidation of polyunsaturated fatty acids (PUFAs). Most oxylipins have signaling functions, especially the oxylipin-derived phytohormone JA, and are involved in the regulation of (a)biotic stress responses as well as plant growth and development (Wasternack and Feussner 2018). Oxylipin biosynthesis is primarily driven by the availability of the substrate fatty acid (FA) either in its free form or esterified to plastid membrane and storage lipids (Feussner et al. 1995, Andersson et al. 2006, Nilsson et al. 2012). Based on our metabolomics analysis, there is an increase in free linolenic acid (18:3, the most abundant FA) in *gnat4* and *gnat10*, while free linoleic acid (FA 18:2) accumulates in the *gnat10* mutant as compared to Col-0 (**Table 2**, **Supplementary Dataset S1**). Similarly, the amount of the most abundant thylakoid membrane lipid MGDG is increased in most *gnat* mutant lines (**Table 1**, **Fig. 4**, **Supplementary Dataset S1**), meaning that the lack of substrate does not seem to be behind the observed decrease in oxylipins. In addition to serving as the precursors of JA, plastid galactolipids MGDG and digalactosyldiacylglycerol (DGDG) also seem to have a role in the regulation of JA biosynthesis. Recent reports have shown that many of the phenotypic traits associated with mutants with an altered MGDG:DGDG ratio are, in fact, caused by changes in the amount of JA (Kelly et al. 2016, Lin et al. 2016, Li and Yu 2018).

The first oxidative step in oxylipin biosynthesis is catalyzed by lipoxygenase (LOX) enzymes that, depending on their positional specificity, are classified into 13-LOX and 9-LOX enzymes (**Fig. 4**). LOX enzymes thus specifically produce C-13- or C-9-oxygenated PUFAs, in contrast to chemical oxygenation by reactive oxygen species that results in a mixture of different positional isomers of FA hydroperoxides (Andreou et al. 2009). Two isomers of HpOTre, an FA hydroperoxide derived from linolenic acid (**Table 1**, **Supplementary Dataset S1**, **Fig. 4**), were markedly decreased in all of the studied *gnat* mutant lines (except *gnat1*) with isomer 2 being by far more abundant. Based on the presence of two distinct isomers of HpOTre, it is conceivable that enzymatic oxygenation by LOX enzymes is behind their formation. Interestingly, LOX2, a 13-LOX enzyme and the predominant LOX enzyme in the leaf, has up to eight lysine

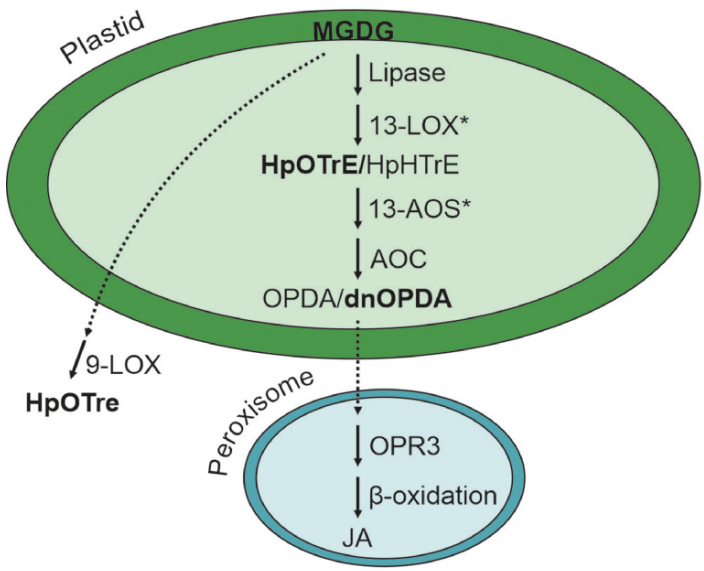

FC (vs. Col-0)	MGDG 18:3/16:3 (1)	18:3/16:3 (2)	18:3/18:3
gnat1	--	--	--
gnat2	1.81	1.35	--
gnat4	2.08	1.42	1.34
gnat7	1.96	--	1.29
gnat10	2.12	1.53	1.56

FC (vs. Col-0)	HpOTrE isomer 3	isomer 2
gnat1	--	--
gnat2	0.60	0.62
gnat4	0.59	0.67
gnat7	0.56	0.61
gnat10	0.56	0.56

FC (vs. Col-0)	dnOPDA
gnat1	--
gnat2	0.60
gnat4	0.69
gnat7	0.62
gnat10	0.57

Fig. 4 The synthesis of the oxylipin-derived JA and the FCs of related metabolites identified in the current study. Enzymes with known acetylation sites are marked with an asterisk. Abbreviations for compounds and enzymes: MGDG, monogalactosyldiacylglycerol; LOX, lipoxygenase; HpOTrE, hydroperoxyl-octadecatrienoic acid; HpHTrE, hydroperoxyl- hexadecatrienoic acid; 13-AOS, 13-allene oxide synthase; AOC, allene oxide cyclase; (dn)OPDA, (dinor-)12-oxophyto-dienoic acid; OPR3, 12-oxophytodienoate reductase 3; JA, jasmonic acid. The figure is based on Wasternack and Feussner (2018).

acetylation sites (Hartl et al. 2017, Wasternack and Feussner 2018, Koskela et al. 2018b), which might indicate that changes in acetylation of the LOX enzymes affect oxylipin production in the *gnat* mutants.

The 13-LOX branch of oxylipin biosynthesis is well characterized, not in the least, because of its important role in JA synthesis (Schaller and Stintzi 2009, Wasternack and Feussner 2018). During JA biosynthesis, the 13-oxygenated PUFA (derived from 18:3 or 16:3 FAs) is converted to an unstable allylic epoxide by 13-allene oxide synthase (AOS) (**Fig. 4**). The allylic epoxide is then converted to a cyclic dnOPDA by allene oxide cyclase (AOC). The precursors for OPDA and dnOPDA are linolenic acid (18:3) and hexadecatrienoic acid (16:3), respectively. The formation of dnOPDA is the last plastid-localized step of JA biosynthesis, which is finalized in the peroxisome by the action of 12-oxophytodienoate reductase 3 (OPR3) and two to three cycles of β-oxidation. Interestingly, the accumulation of dnOPDA was decreased in all studied *gnat* mutant lines except *gnat1* (**Table 1**, **Supplementary Dataset S1**, **Fig. 4**). The decrease in dnOPDA could be a reflection of a decrease in oxylipins upstream of dnOPDA, but unfortunately no other hexadecatrienoic acid–derived oxylipins were identified in our analysis. In addition to their role as JA precursors, both dnOPDA and OPDA have, at least partially overlapping, signaling functions of their own (Stintzi et al. 2001, Taki et al. 2005, Buseman et al. 2006, Dave et al. 2011). However, most of the available research focuses on OPDA, which likely due to the higher availability of its precursor PUFA (18:3) is more abundant than dnOPDA.

There is strong evidence suggesting that JA biosynthesis is regulated on a post-translational level (Scholz et al. 2015), but the mechanism behind this regulation has remained elusive. Intriguingly, the only isoform of AOS, the plastid enzyme that catalyzes the first committed step of JA biosynthesis, has up to seven lysine acetylation sites (Hartl et al. 2017, Koskela et al. 2018b), whose function is yet unknown. Based on the decrease in dnOPDA observed in our metabolomics analysis, it is tempting to speculate that acetylation might be involved in the enigmatic post-translational regulation of JA.

Deficiency of chloroplast GNATs results in the increased accumulation of Rubisco and RCA in the thylakoid fraction

Several studies have linked lysine acetylation to carbon assimilation through the adjustment of Rubisco activity either directly or by altering the activity of RCA (Finkemeier et al. 2011, Gao et al. 2016, Hartl et al. 2017). Rubisco, the most abundant enzyme in plants, catalyzes the first step of carbon assimilation reactions in the soluble stroma of the chloroplast. Nevertheless, several reports have suggested that the organization of the carbon assimilation enzymes into thylakoid-associated multienzyme complexes might facilitate carbon assimilation (Suss et al. 1993, Sainis et al. 2003, Dani and Sainis 2005, Agarwal et al. 2009). As acetylation affects the charge of the protein and thereby potential interactions (Drazic et al. 2016), the increased association of Rubisco to the thylakoid membrane (**Fig. 2C**,

Supplementary Fig. S7) may result from the differential acetylation status of proteins in the *gnat* mutants as compared to Col-0 (Koskela et al. 2018b, Bienvenut et al. 2020). This hypothesis is supported by the fact that Rubisco is the most heavily acetylated protein in the chloroplast (Finkemeier et al. 2011, Wu et al. 2011, Hartl et al. 2017). Another possibility is that potential changes in Rubisco acetylation alter its activity and lead to the observed reallocation of Rubisco as a way to maintain normal Rubisco function. In support of this, changes in the lysine acetylation status of Rubisco have been linked to enzyme activity (Finkemeier et al. 2011, Gao et al. 2016, Hartl et al. 2017), although the exact mechanism remains unclear. However, the involvement of lysine acetylation in the regulation of Rubisco has also been challenged due to the low stoichiometry of acetylation events in 6-week-old *Arabidopsis* rosettes (O'Leary et al. 2020). Based on our results, it seems likely that the membrane recruitment of Rubisco is affected by changes in acetylation, but these changes are not reflected in the net carbon assimilation efficiency of the plants (**Fig. 2**, **Supplementary Fig. S9**).

In the dark, Rubisco is inhibited by the binding of sugar phosphate–like molecules that are removed from Rubisco active sites upon the RCA-driven, light-induced conformational change of the enzyme. RCA, on the other hand, requires ATP to function and is inhibited by the ADP formed upon Rubisco activation. Increased lysine acetylation of RCA has been shown to decrease its sensitivity to ADP inhibition, thus increasing its ability to activate Rubisco (Hartl et al. 2017). Additionally, it has been suggested that RCA is recruited to the thylakoid membrane upon Rubisco activation, possibly in its inactive, ADP-bound form (Chen et al. 2010). The release of RCA from the thylakoids depends on the formation of the proton gradient across the thylakoid membrane (ΔpH) and increasing ATP levels (Chen et al. 2010). Interestingly, the amount of RCA is markedly increased in the thylakoid fraction of several *gnat* mutants (**Fig. 2C**, **Supplementary Fig. S7**), although ΔpH is unaffected (**Supplementary Dataset S3**). Based on our experiments, it is not possible to assess the amount of ATP in the chloroplast stroma, but unchanged *pmf* and ATP synthase conductivity in the *gnat* mutants suggest that there are no major differences in ATP production as compared to Col-0 (**Supplementary Dataset S3**). However, the amount of ATPase subunits ATP-β and ATP-f is slightly decreased in the *gnat6* and *gnat4* mutants, respectively (**Fig. 2B**, **Supplementary Fig. S8**), indicating that changes in ATP production cannot be ruled out. One possible explanation for the high accumulation of RCA in the thylakoid fraction of *gnat* mutants (**Fig. 2C**, **Supplementary Fig. S7**) could be that the potential decrease in the acetylation of RCA increases its affinity to ADP, thereby enhancing thylakoid recruitment. However, this hypothesis requires further investigation, which is beyond the scope of this study. Because no increase was observed in the amount of FNRL, a stromal oxidoreductase, and FNR in the thylakoid fraction of the *gnat* mutants, the increase of both Rubisco and RCA may suggest that acetylation specifically affects the allocation of the enzymes involved in carbon assimilation. Whether the acetylation and/or allocation of these enzymes have physiological consequences remains a topic for further studies.

Chloroplast acetyltransferases and photosynthesis

One of the most pronounced consequences of the GNAT knock-out on the plant metabolome was the low content of ascorbate in *gnat2*, *gnat4*, *gnat7* and *gnat10* (**Table 1**, **Supplementary Dataset S1**). Ascorbate plays an important role in various photosynthesis-related processes in chloroplasts. Ascorbate, along with low pH, is required for the activity of VDE, which converts violaxanthin to antheraxanthin and zeaxanthin upon the acclimation of plants to HL (Müller-Moulé et al. 2002, 2004). The accumulation of zeaxanthin and the conformational change in the lumenal PSBS protein result in the induction of NPQ, which protects the photosynthetic machinery upon the exposure of the plant to intense illumination (Jahns and Holzwarth 2012). Despite the decrease in the ascorbate content, no differences were recorded in the accumulation of xanthophyll cycle pigments or NPQ-related proteins VDE and PSBS, or in the dynamics of the xanthophyll cycle between the *gnat* mutants and Col-0 (**Supplementary Fig. S6**). Similarly, under low-light conditions, the content of xanthophyll cycle pigments and photosynthetic properties did not differ between the ascorbate-deficient *vtc2* mutants and Col-0 (Müller-Moulé et al. 2004). Since only the *gnat2* plants showed any changes in NPQ (**Table 3**, **Supplementary Dataset S2**, Koskela et al. 2018b), it is likely that not the ascorbate content but rather some other changes specific to *gnat2*, such as previously described decreased acetylation of various thylakoid proteins or compact stacking of thylakoid grana (Koskela et al. 2018b, Rantala et al. 2022), have an impact on NPQ in *gnat2*.

In addition to the induction of NPQ, ascorbate is also an important component in the quenching of photoproduced superoxide and hydrogen peroxide (water–water cycle and Foyer–Halliwell–Asada cycle) and thus is crucial for HL acclimation (Asada 1999). Reactive oxygen species damage the D1 protein of PSII, which must be degraded, resynthesized and inserted in the thylakoid-embedded PSII in a multistep process known as the PSII repair cycle (Aro et al. 1993). Importantly, the phosphorylation of the D1 protein plays a central role in the regulation of PSII repair (Baena-González et al. 1999, Mulo et al. 2008). The reduced ascorbate content and changes in thylakoid protein phosphorylation suggest that the PSII repair cycle might be affected by the loss of GNAT enzymes. However, this was clearly not the case since none of the *gnat* mutants showed enhanced susceptibility to photoinhibition or any differences in the D1 protein content between the *gnat* mutants and Col-0 (**Fig. 3**). Apparently, the *gnat* plants have adopted other, yet unidentified ascorbate-independent strategies to avoid HL-induced stress.

The only visible phenotype observed among the *gnat* mutants was the light-dependent growth retardation of the *gnat2* mutant. A similar light-dependent effect on *gnat2* growth was also observed by Lee and Back (2021), where slight growth retardation was visible when plants were grown at a PPFD of

100 μmol m^{-2} s^{-1} and the effect increased in plants grown under a PPFD of 50 μmol m^{-2} s^{-1}. Interestingly, Lee and Back (2021) used a different *gnat2* (SALK_020577) mutant than us, thus providing further support to our results. Since *gnat2* growth appears to be affected under conditions where state transitions usually take place (relatively low light and fluctuating light) (**Fig. 1B**, **Supplementary Fig. S5**, Koskela et al. 2020, Lee and Back 2021), it seems likely that impaired state transitions are behind the retarded growth phenotype specific to *gnat2*. However, under constant light conditions used in our experiments, the phenotype seems to be very sensitive even to small changes in light intensity.

Can the GNATs acetylate metabolites?

The ability of GNAT1 and GNAT2 to function as protein and metabolite acetyltransferases raises the question whether any of the remaining plastid GNATs have metabolite acetyltransferase activity. Although our metabolomic analysis does not directly answer this question, the striking decreases in N_{α}-acetyl-L-arginine in *gnat2* and *N*-acetylproline in *gnat7* (**Table 2**, **Supplementary Dataset S1**) give reasons to speculate about the involvement of these two GNATs in the acetylation of free amino acids. One alternative explanation for the presence (or in our case lack) of N-terminally acetylated amino acids would be that their acetylation takes place when the amino acid is attached to the N-terminus of a peptide, prior to its cleavage during N-terminal processing. However, since arginine and proline are not among the preferred N-terminally acetylated amino acids for GNAT2 and GNAT7 (Bienvenut et al. 2020), this option does not seem to be a cause for the changed level of acetylated amino acids in *gnat2* and *gnat7*. Additionally, due to the relaxed NAT specificity of the plastid GNATs, one would expect to see changes in the abundance of the acetylated amino acids in several *gnat* mutant lines as opposed to a very strong decrease specific to one line. The possibility of GNATs being able to acetylate free amino acids is somewhat supported by the existence of Hpa3, a yeast *Saccharomyces cerevisiae* GNAT, that catalyzes the acetylation of proteins and D-amino acids in the process of their detoxification (Yow et al. 2004, 2006, Sampath et al. 2013).

Very little to nothing is known about the physiological role and prevalence of free acetylated arginine and proline in plants, which were strikingly decreased in *gnat2* and *gnat7* plants, respectively (**Table 2**). In mammals, N_{α}-acetyl-L-arginine has been shown to accumulate when the urea cycle is impaired, and some studies have implicated N_{α}-acetyl-L-arginine in oxidative stress, although the mechanism behind this remains elusive (Sasso et al. 2014, Chaleckis et al. 2016, Olesova et al. 2020). Proline itself has a well-known function as an osmoprotectant that accumulates in plants under different stresses (Verbruggen and Hermans 2008), but no reports on *N*-acetylproline have been found.

Taken together, our results show that the chloroplast GNATs, known to possess both NAT and KAT activities, have a marked effect on the plant metabolome. It will be intriguing to resolve whether these effects are solely indirect and result from chloroplast protein acetylation or whether the GNATs are also able to act in the acetylation of metabolites, such as amino acids. The limited effect of *gnat* knock-outs on photosynthesis and the shared metabolome features of the *gnat* mutants together with the relaxed substrate specificity of GNATs observed by Bienvenut et al. (2020) indicate that the function of the GNAT enzymes is at least partly overlapping. An especially interesting topic for future research is the effect the GNATs have on Rubisco and RCA. Future research will also reveal the impact of double or multiple *gnat* knock-outs on the acetylation status of proteins, the accumulation of metabolites and the physiological responses of the plants.

Materials and Methods

Growth conditions and *gnat* mutant screening

Arabidopsis thaliana Col-0 and mutant plants were grown on a peat:vermiculite mixture (2:1) under 8-h light/16-h dark cycles at a PPFD of 130 μmol m^{-2} s^{-1} (Osram Powerstar HQI®-BT 400 W/D PRO Daylight, OSRAM GmbH, Munich, Germany), +23°C and a relative humidity of 50% for 4–6 weeks, as indicated. Plants for biological replicates were grown at different times on separate trays. For some experiments, plants were grown under different PPFDs, as indicated.

Seed stocks for the *gnat* T-DNA lines were obtained from the Nottingham Arabidopsis Stock Centre and were PCR-screened according to Salk Institute Genomic Analysis Laboratory instructions using the primers listed in **Supplementary Table S1**. The *gnat2* line (*nsi-1*, SALK_033944) was screened by Koskela et al. (2018b). The absence/presence of *gnat* mRNA was confirmed by end-point RT-PCR for *gnat1* (SALK_150736), *gnat4* (SALK_037490), *gnat5* (GABI_034E09), *gnat7* (SAIL_273_E06) and *gnat10* (SALK_012435). The amount of mRNA in *gnat3.1* (SALK_204085), *gnat3.2* (GABI_809D05) and *gnat6* (SALK_035208) was evaluated with quantitative real-time PCR using the IQ SYBR Green Supermix (annealing at 61.4°C) and the IQ™5 Cycler (Bio-Rad, Hercules, California, USA). All mRNA was extracted using the innuPrep Plant RNA Kit (Analytik Jena™, Jena, Germany), followed by a DNase treatment with the TURBO DNA-free™ Kit (Invitrogen™, Waltham, Massachusetts, USA) and cDNA synthesis with the iScript™ cDNA synthesis kit (Bio-Rad) according to the manufacturer's instructions. Primers used for the end-point RT-PCR and quantitative real-time PCR are listed in **Supplementary Table S1**.

Pigment analyses

For total Chl determination, weighed 0.636 cm^2 leaf discs from 5-week-old plants grown at a PPFD of 140–150 μmol m^{-2} s^{-1} were incubated in 1 ml of N,N-dimethylformamide (DMF) in darkness for 16 h. Following 5-min centrifugation at 18,000×*g*, absorbance was measured at 646.6, 663.6 and 750 nm and used to calculate the total Chl *a* and *b* content with the following equations: Chl $a = 12.7 * (A_{663.6} - A_{750}) - 2.79 (A_{646.6} - A_{750})$ and Chl $b = 20.7 * (A_{646.6} - A_{750}) - 4.62 (A_{663.6} - A_{750})$ (Inskeep and Bloom 1985).

Xanthophyll pigment analysis

Pigments (zeaxanthin, violaxanthin and antheraxanthin) were extracted from 5-week-old *Arabidopsis* leaf discs (diameter 8 mm, frozen in liquid N_2 and ground). Of 100% MeOH at −80°C, 300 μl was added, and the samples were centrifuged at 18,500×*g* for 15 min at −5°C. The supernatant was centrifuged (18,500×*g*, 10 min, −5°C) to pellet the leaf debris and then filtered through a syringe-driven filter (Millex, Rahway, New Jersey, USA). The pigments were separated by HPLC according to Gilmore and Yamamoto (1991) using a reverse-phase C18 column (LiChroCART 125-4; Hewlett Packard, Palo Alto, California, USA), a series 1100 HPLC device with a diode array and a fluorescence detector (Agilent Technologies, Palo Alto, California, USA). A constant flow rate of 500 μl min^{-1} was used. The program started with a 4-min isocratic run with buffer A [acetonitrile–methanol–Tris-HCl buffer 0.1 M (72:8:3, v/v), pH 8.0] followed by a linear gradient from 0% buffer B to 100% buffer B (methanol–hexane 4:1 v/v).

The isocratic run of buffer B lasted 19 min. The column was re-equilibrated between samples for 40 min with buffer A. Pigments were detected at 440 nm. Pigment standards were supplied by DHI Lab products (Hørsholm, Denmark).

Metabolomics

Of frozen leaf samples, 100 mg was homogenized in 600 µl of cold methanol (80% v/v) and centrifuged (17,949xg, +4°C, 10 min). After the centrifugation, 100 µl of supernatant was collected into separate tubes and 400 µl cold methanol (80% v/v) was added, after which the supernatant was filtered (Acrodisc 0.2-µm polytetrafluoroethylene (PTFE) membrane; Pall, Port Washington, New York, USA) into HPLC vials for analysis.

The samples were analyzed by LC–MS, consisting of a Vanquish Flex UHPLC system (Thermo Scientific, Bremen, Germany) coupled with a high-resolution Orbitrap mass spectrometer (Q Exactive Focus; Thermo Scientific). The analytical method has been described in more detail by Hanhineva et al. (2015) and Klåvus et al. (2020). In brief, a Zorbax Eclipse XDB-C18 column (2.1 × 100 mm, 1.8 µm; Agilent Technologies) was used for the reversed-phase separation and an Aqcuity UPLC BEH amide column (Waters, Milford, Massachusetts, USA) for hydrophilic interaction liquid chromatography separation. After each chromatographic run, the ionization was carried out using jet stream electrospray ionization (ESI) in the positive and negative modes, yielding four data files per sample. The collision energies for the MS/MS analysis were selected as 10, 20 and 40 V for compatibility with spectral databases.

Peak detection and alignment were performed in MS-DIAL ver. 4.60 (Tsugawa et al. 2015). For the peak collection, *m*/*z* values were between 50 and 1,500, and all retention times were considered. The amplitude of the minimum peak height was set at 250,000. The peaks were detected using the linear weighted moving average algorithm. For the alignment of the peaks across samples, the retention time tolerance was 0.05 min, and the *m*/*z* tolerance was 0.015 Da.

Differential features between the genotypes were detected using feature-wise linear mixed models, where feature levels were predicted by genotype and series was used as a random effect. All the *P*-values were corrected using the Benjamini–Hochberg false discovery rate (FDR). The corrected *P*-values (*q*-values) > 0.1 were considered significant.

The chromatographic and mass spectrometric characteristics (retention time, exact mass and MS/MS spectra) of the significantly differential molecular features were compared with entries in an in-house standard library and publicly available databases, such as METLIN and The Human Metabolme Database, as well as with the published literature. The annotation of each metabolite and the level of identification were given based on the recommendations published by the Chemical Analysis Working Group Metabolomics Standards Initiative (Sumner et al. 2007).

Detection of melatonin

The frozen plant material was homogenized using a ball mill (Retsch, Haan, Germany) and extracted with 1 ml of methanol twice in darkness to prevent melatonin degradation in light. Ultrasonication of the samples (20 min, +4°C) was used to assist and accelerate the extraction of melatonin. The extracts were centrifuged, filtered, evaporated to dryness and reconstituted in 100 µl methanol prior to the UPLC–MS analysis. The analyses were executed using the Waters Acquity® UPLC system (Waters) attached to Waters Synapt G2 HDMS mass spectrometer (Waters) via an ESI ion source. Samples were analyzed in positive, sensitivity ion mode. The mass range was set from 80 to 600. Separation was performed by injecting 3 µl of plant extract into Acquity® UPLC BEH C18 column (1.7 µm, 50 × 2.1 mm; Waters) at +35°C.

The mobile phase consisted of 0.1% formic acid in both (A) H_2O and (B) acetonitrile (Chromasolv® grade; Sigma-Aldrich, Munich, Germany). A linear gradient started at 97% of A and decreased to 30% in 5 min. The flow rate of the mobile phase was 0.6 ml min^{-1}, and the tray temperature was set to +12°C. The capillary voltage, sampling cone, extraction cone, source temperature, desolvation temperature, cone gas flow rate and desolvation gas flow rate were set to 3.0 kV, 30, 3.0, 120°C, 360°C, 20 l h^{-1} and 800 l h^{-1}, respectively. The melatonin concentration was determined by using the calibration curve of the melatonin standard (Sigma-Aldrich), and the results were normalized to fresh weight [FW (g)].

Protein isolation

Thylakoid proteins were isolated from fresh 5-week-old leaves grown at a PPFD of 130 µmol m^{-2} s^{-1} that were ground in cold buffer (300 mM sucrose, 50 mM HEPES-KOH, pH 7.6, 5 mM $MgCl_2$, 1 mM Na-EDTA, 1.25% bovine serum albumin, 22 mM ascorbate and 10 mM NaF). Thylakoids from HL-treated plants were isolated after a 2-h treatment at a PPFD of 1,000 µmol m^{-2} s^{-1}. The homogenate was filtered through Miracloth (Millipore, Burlington, Massachusetts, USA) and centrifuged at 4,000×*g* for 6 min at 4°C. The pellet was resuspended in a hypotonic lysis buffer [5 mM sucrose, 10 mM HEPES-KOH, pH 7.6, 5 mM $MgCl_2$, 10 mM NaF and Pierce protease inhibitor (Thermo Scientific)] to break the chloroplasts, and the suspension was centrifuged at 4,000×*g* for 6 min at 4°C. The pellet was washed by resuspending in the storage buffer (100 mM sucrose, 10 mM HEPES-KOH, pH 7.6, 10 mM $MgCl_2$ and 10 mM NaF) and centrifuged at 10,000×*g* for additional 6 min at 4°C. Finally, the pellet containing the thylakoids was resuspended in the storage buffer. The total Chl content was determined according to Porra et al. (1989).

For total protein extraction, leaves from 5-week-old plants were homogenized in liquid N_2 and suspended in the protein extraction buffer (100 mM Tris-HCl, pH 8.0, 50 mM Na-EDTA, 0.25 mM NaCl, 0.75% SDS, 1 mM DTT). The samples were incubated for 10 min at 68°C and centrifuged twice at 18,400×*g* for 10 min at 22°C. The supernatant was collected, and the total Chl content was determined according to Porra et al. (1989).

Protein analyses using gel-based methods

BN gels, 2D gels and samples were prepared as described by Rantala et al. (2018). Thylakoid samples were solubilized with 1% digitonin or β-dodecyl maltoside, and samples containing 5 µg of Chl were separated on BN gels. For staining, the gels were incubated in a fix solution (40% methanol and 10% acetic acid) for at least 1 h, stained with Coomassie (0.1% Coomassie R-250, 40% methanol and 10% acetic acid) for 30 min, followed by a 15-min incubation in the fix solution. Finally, the gels were incubated in Milli-Q water for at least 16 h before imaging with Geliance 1,000 (Perkin Elmer, Waltham, Massachusetts, USA). For the detection of phosphoproteins and total proteins from SDS gels, Pro-Q™ Diamond phosphoprotein gel stain (Invitrogen) and SYPRO Ruby protein gel stain (Invitrogen) were used according to the manufacturer's instructions.

For immunoblot analysis, protein samples (thylakoid/total) were solubilized in the Laemmli buffer (Laemmli 1970) supplemented with 6 M urea, and 0.06–5 µg of Chl was separated on 12% acrylamide gels containing 6 M urea. The proteins were blotted onto an Immobilon-FL or Immobilon-P membrane (Merck Millipore, Darmstadt, Germany), blocked with 5% milk in Tris Buffered Saline with Tween (TTBS) (20 mM Tris-HCl, pH 7.5, 150 mM NaCl and 0.05% Tween 20) and incubated with the primary antibody for 16 h. The membrane was washed 4 × 5 min with TTBS and incubated with IRDye® 800CW Goat anti-Rabbit IgG secondary antibody (1:20,000 in 1% milk/TTBS; LI-COR, Lincoln, Nebraska, USA) or enhanced chemiluminescence (ECL) Anti-rabbit IgG HRP (1:10,000 in 1% milk/TTBS, NA9340V; GE Healthcare, Chicago, Illinois, USA). After 3 × 5 min washes with TTBS and 2 × 5 min washes with TBS (20 mM Tris-HCl, pH 7.5, 150 mM NaCl), the membranes were imaged with LI-COR Odyssey CLx or incubated in ECL (Amersham, Marlborough, Massachusetts, USA) for 5 min and developed on Super RX-N x-ray films (Fujifilm, Tokyo, Japan). The antibodies, their dilutions, the amount of protein used and the detection method are listed in **Supplementary Table S2**.

Carbon assimilation measurements

Carbon assimilation was measured using 5-week-old plants grown at a PPFD of 160 µmol m^{-2} s^{-1} with the GFS-3000 gas exchange system (Walz, Effeltrich, Germany) equipped with a standard measuring head 3,010 M and an LED light source 3,041 L. Measurements were performed on 5–6 plants/line at a constant

humidity of 14,000 ppm, and the cuvette temperature was set to 23°C. For the light and CO_2 response curves, CO_2 assimilation and H_2O evaporation were monitored at different light intensities (PPFD steps of 170, 150, 125, 100, 75, 50, 170, 250, 500, 750 and 1,000 μmol m^{-2} s^{-1}) and CO_2 concentrations (400, 100, 200, 300, 400, 700, 1,000 and 2,000 ppm), respectively. In the light response measurement, the CO_2 concentration was 400 ppm, while in the CO_2 response measurement, the light intensity was set to a PPFD of 170 μmol m^{-2} s^{-1}.

DUAL-PAM measurements

Light curve and ECS measurements were performed using 6-week-old plants grown at a PPFD of 130 μmol m^{-2} s^{-1} using DUAL-PAM-100 (Walz) equipped with DUAL-E emitter and DUAL-DR detector units as described by Koskela et al. (2018a). The plants were incubated in the dark for 30 min and exposed to 5-min illumination steps at the PPFDs of 50, 75, 100, 125, 150, 250, 500, 700 and 1,000 μmol m^{-2} s^{-1}. The measurement was performed on 3–4 plants/line.

The magnitude and partitioning of *pmf* were evaluated by measuring the light-induced absorbance difference between 550 and 515 nm (ECS) using a DUAL-PAM-100 spectrometer equipped with the P515/535 accessory module (Schreiber and Klughammer 2008) with the measuring light at 500–1,000 Hz pulse frequency. Plants were dark acclimated for 30 min, and a saturating pulse (20 μs at 8,000 μmol m^{-2} s^{-1}) to determine the maximal ECS change, followed by 3-min steps of increasing red actinic light intensities of 60, 125 and 500 μmol photons m^{-2} s^{-1}. Each light step was followed by 1 min of darkness to monitor the post-illumination response of ECS. Additionally, after 2 min at each light intensity, the plants were subjected to 10 short flashes of darkness (250 ms) to probe ATPase conductivity. The measured values were normalized using the maximal ECS change, and the partitioning of *pmf* to ΔpH and $\Delta\Psi$ and the proton flux (vH^+) and conductivity (gH^+) were determined as described by Schreiber and Klughammer (2008). The measurement was performed on 6 plants/line.

Photoinhibition

For the photoinhibition experiment, detached leaves from 5–6-week-old plants grown at a PPFD of 130–140 μmol m^{-2} s^{-1} were floated on water or 2.3 nM lincomycin for 16 h and moved to an HL of 600 μmol photons m^{-2} s^{-1} (Heliospectra DYNA, 530 nm and white 5700K LED) for 2 h. After the HL treatment, the leaves in water were moved to GL (130 μmol photons m^{-2} s^{-1}) for recovery. During the experiment, samples were collected at time points of 0 h, 1-h HL, 2-h HL, 0.5-h GL and 1.5-h GL. The quantum yield of PSII was monitored by measuring F_v/F_m using a FluorPen (Photon Systems Instruments, Drásov, Czech Republic) from five to six leaves incubated in the dark for 15–20 min. For the immunoblot analysis, total protein was extracted as described previously.

Statistical analyses

Statistical analysis was performed using IBM SPSS Statistics software using one-way ANOVA, and when applicable, followed by Tukey's post hoc test with $P < 0.05$ cutoff.

Supplementary Data

Supplementary data are available at *PCP* online.

Data Availability

All data supporting the findings of this study are available within the manuscript and its supplementary data published online.

Funding

Academy of Finland (321616, 330083); Doctoral Programme in Molecular Life Sciences (University of Turku, Finland); Deutscher Akademischer Austauschdienst (DAAD) Programme for Project-Related Personal Exchange; European Research Area-Coordinated Action in Plant Sciences (ERA-CAPS) Research Programme 'KatNat'.

Acknowledgments

We thank Dr. Saijaliisa Kangasjärvi for the critical reading of the manuscript. We also thank Dr. Esa Tyystjärvi and Tapio Lempiäinen for their generous advice and Maisa Pikkarainen for technical assistance. Metabolomic analysis was performed by Afekta Technologies Ltd. (Finland), and melatonin determination was performed in the Viikki Metabolomics Unit in the Metabo-HiLIFE platform (University of Helsinki, Finland). We acknowledge the Finnish Infrastructure for Photosynthesis Research PHOTOSYN for its excellent research facilities.

Author Contributions

P.M. and I.F. assisted with the conceptualization; A.I., M.R., L.L., M.M.K., N.S. and J.S.M. assisted with the investigation; A.I. assisted with the formal analysis; P.M. and I.F. assisted with the resources; A.I. and P.M. assisted with the writing—original draft; M.R. and I.F. assisted with the writing—review & editing; A.I. assisted with the visualization and P.M. and I.F. assisted with the supervision and funding acquisition.

Disclosures

The authors have no conflicts of interest to declare.

References

Agarwal, R., Ortleb, S., Sainis, J.K. and Melzer, M. (2009) Immunoelectron microscopy for locating Calvin cycle enzymes in the thylakoids of *Synechocystis* 6803. *Mol. Plant* 2: 32–42.

Aksnes, H., Ree, R. and Arnesen, T. (2019) Co-translational, post-translational, and non-catalytic roles of N-terminal acetyltransferases. *Mol. Cell* 73: 1097–1114.

Andersson, M.X., Hamberg, M., Kourtchenko, O., Brunnström, Å., McPhail, K.L., Gerwick, W.H., et al. (2006) Oxylipin profiling of the hypersensitive response in *Arabidopsis thaliana*. *J. Biol. Chem.* 281: 31528–31537.

Andreou, A., Brodhun, F. and Feussner, I. (2009) Biosynthesis of oxylipins in non-mammals. *Prog. Lipid Res.* 48: 148–170.

Aro, E.M., Suorsa, M., Rokka, A., Allahverdiyeva, Y., Paakkarinen, V., Saleem, A., et al. (2005) Dynamics of photosystem II: a proteomic approach to thylakoid protein complexes. *J. Exp. Bot.* 56: 347–356.

Aro, E.M., Virgin, I. and Andersson, B. (1993) Photoinhibition of photosystem II. Inactivation, protein damage and turnover. *Biochim. Biophys. Acta Bioenerg.* 1143: 113–134.

Asada, K. (1999) The water-water cycle in chloroplasts: scavenging of active oxygens and dissipation of excess photons. *Annu. Rev. Plant Physiol. Plant Mol. Biol.* 50: 601–639.

Baena-González, E., Barbato, R. and Aro, E.M. (1999) Role of phosphorylation in the repair cycle and oligomeric structure of photosystem II. *Planta* 208: 196–204.

Benz, J.P., Stengel, A., Lintala, M., Lee, Y.H., Weber, A., Philippar, K., et al. (2009) *Arabidopsis* Tic62 and ferredoxin-NADP(H) oxidoreductase form light-regulated complexes that are integrated into the chloroplast redox poise. *Plant Cell* 21: 3965–3983.

Bienvenut, W.V., Brünje, A., Boyer, J., Mühlenbeck, J.S., Bernal, G., Lassowskat, I., et al. (2020) Dual lysine and N-terminal acetyltransferases reveal the complexity underpinning protein acetylation. *Mol. Syst. Biol.* 16: 1–23.

Bienvenut, W.V., Sumpton, D., Martinez, A., Lilla, S., Espagne, C., Meinnel, T., et al. (2012) Comparative large scale characterization of plant versus mammal proteins reveals similar and idiosyncratic N-α-acetylation features. *Mol. Cell Proteomics* 11: 1–14.

Böttcher, C., Chapman, A., Fellermeier, F., Choudhary, M., Scheel, D. and Glawischnig, E. (2014) The biosynthetic pathway of indole-3-carbaldehyde and indole-3-carboxylic acid derivatives in *Arabidopsis*. *Plant Physiol.* 165: 841–853.

Buseman, C.M., Tamura, P., Sparks, A.A., Baughman, E.J., Maatta, S., Zhao, J., et al. (2006) Wounding stimulates the accumulation of glycerolipids containing oxophytodienoic acid and dinor-oxophytodienoic acid in *Arabidopsis* leaves. *Plant Physiol.* 142: 28–39.

Chaleckis, R., Murakami, I., Takada, J., Kondoh, H. and Yanagida, M. (2016) Individual variability in human blood metabolites identifies age-related differences. *Proc. Natl. Acad. Sci. U.S.A.* 113: 4252–4259.

Chen, J., Wang, P., Mi, H.L., Chen, G.Y. and Xu, D.Q. (2010) Reversible association of ribulose-1, 5-bisphosphate carboxylase/oxygenase activase with the thylakoid membrane depends upon the ATP level and pH in rice without heat stress. *J. Exp. Bot.* 61: 2939–2950.

Dani, D.N. and Sainis, J.K. (2005) Isolation and characterization of a thylakoid membrane module showing partial light and dark reactions. *Biochim. Biophys. Acta Biomembr.* 1669: 43–52.

Dave, A., Hernández, M.L., He, Z., Andriotis, V.M.E., Vaistij, F.E., Larson, T.R., et al. (2011) 12-oxo-phytodienoic acid accumulation during seed development represses seed germination in *Arabidopsis*. *Plant Cell* 23: 583–599.

Dinh, T.V., Bienvenut, W.V., Linster, E., Feldman-Salit, A., Jung, V.A., Meinnel, T., et al. (2015) Molecular identification and functional characterization of the first Nα-acetyltransferase in plastids by global acetylome profiling. *Proteomics* 15: 2426–2435.

Drazic, A., Myklebust, L.M., Ree, R. and Arnesen, T. (2016) The world of protein acetylation. *Biochim. Biophys. Acta Proteins Proteomics.* 1864: 1372–1401.

Feussner, I., Wasternack, C., Kindl, H. and Kühn, H. (1995) Lipoxygenase-catalyzed oxygenation of storage lipids is implicated in lipid mobilization during germination. *Proc. Natl. Acad. Sci. U.S.A.* 92: 11849–11853.

Finkemeier, I., Laxa, M., Miguet, L., Howden, A.J.M. and Sweetlove, L.J. (2011) Proteins of diverse function and subcellular location are lysine acetylated in *Arabidopsis*. *Plant Physiol.* 155: 1779–1790.

Gao, X., Hong, H., Li, W.C., Yang, L., Huang, J., Xiao, Y.L., et al. (2016) Down-regulation of Rubisco activity by non-enzymatic acetylation of RbcL. *Mol. Plant* 9: 1018–1027.

Gilmore, A.M. and Yamamoto, H.Y. (1991) Resolution of lutein and zeaxanthin using a non-endcapped, lightly carbon-loaded C18 high-performance liquid chromatographic column. *J. Chromatogr. A* 543: 137–145.

Hanhineva, K., Lankinen, M.A., Pedret, A., Schwab, U., Kolehmainen, M., Paananen, J., et al. (2015) Nontargeted metabolite profiling discriminates diet-specific biomarkers for consumption of whole grains, fatty fish, and bilberries in a randomized controlled trial. *J. Nutr.* 145: 7–17.

Hartl, M., Füßl, M., Boersema, P.J., Jost, J., Kramer, K., Bakirbas, A., et al. (2017) Lysine acetylome profiling uncovers novel histone deacetylase substrate proteins in *Arabidopsis*. *Mol. Syst. Biol.* 13: 949.

Hoshiyasu, S., Kohzuma, K., Yoshida, K., Fujiwara, M., Fukao, Y., Yokota, A., et al. (2013) Potential involvement of N-terminal acetylation in the quantitative regulation of the ε subunit of chloroplast ATP synthase under drought stress. *Biosci. Biotechnol. Biochem.* 77: 998–1007.

Inskeep, W.P. and Bloom, P.R. (1985) Extinction coefficients of chlorophyll a and B in n,n-dimethylformamide and 80% acetone. *Plant Physiol.* 77: 483–485.

Jahns, P. and Holzwarth, A.R. (2012) The role of the xanthophyll cycle and of lutein in photoprotection of photosystem II. *Biochim. Biophys. Acta Bioenerg.* 1817: 182–193.

Kelly, A.A., Kalisch, B., Hölzl, G., Schulze, S., Thiele, J., Melzer, M., et al. (2016) Synthesis and transfer of galactolipids in the chloroplast envelope membranes of *Arabidopsis thaliana*. *Proc. Natl. Acad. Sci. U.S.A.* 113: 10714–10719.

Klåvus, A., Kokla, M., Noerman, S., Koistinen, V.M., Tuomainen, M., Zarei, I., et al. (2020) "Notame": workflow for non-targeted LC–MS metabolic profiling. *Metabolites* 10: 135.

Koskela, M.M., Brünje, A., Ivanauskaite, A., Grabsztunowicz, M., Lassowskat, I., Neumann, U., et al. (2018a) Chloroplast acetyltransferase NSI is required for state transitions in *Arabidopsis thaliana*. *Plant Cell* 30: 1695–1709.

Koskela, M.M., Brünje, A., Ivanauskaite, A., Lopez, L.S., Schneider, D., DeTar, R.A., et al. (2020) Comparative analysis of thylakoid protein complexes in state transition mutants *nsi* and *stn7*: focus on PSI and LHCII. *Photosynth. Res.* 145: 15–30.

Koskela, M.M., Dahlström, K.M., Goñi, G., Lehtimäki, N., Nurmi, M., Velazquez-Campoy, A., et al. (2018b) *Arabidopsis* FNRL protein is an NADPH-dependent chloroplast oxidoreductase resembling bacterial ferredoxin-NADP+ reductases. *Physiol. Plant.* 162: 177–190.

Laemmli, U.K. (1970) Cleavage of structural proteins during the assembly of the head of bacteriophage T4. *Nature* 227: 680–685.

Lee, H.Y. and Back, K. (2018) Melatonin induction and its role in high light stress tolerance in *Arabidopsis thaliana*. *J. Pineal Res.* 65: 1–13.

Lee, H.Y. and Back, K. (2021) Melatonin regulates chloroplast protein quality control via a mitogen-activated protein kinase signaling pathway. *Antioxidants* 10: 511.

Lee, H.Y., Byeon, Y., Lee, K., Lee, H.J. and Back, K. (2014) Cloning of *Arabidopsis* serotonin N-acetyltransferase and its role with caffeic acid O-methyltransferase in the biosynthesis of melatonin in vitro despite their different subcellular localizations. *J. Pineal Res.* 57: 418–426.

Lee, H.Y., Lee, K. and Back, K. (2019) Knockout of *Arabidopsis* serotonin N-acetyltransferase-2 reduces melatonin levels and delays flowering. *Biomolecules* 9: 1–12.

Lin, Y.T., Chen, L.J., Herrfurth, C., Feussner, I. and Li, H.M. (2016) Reduced biosynthesis of digalactosyldiacylglycerol, a major chloroplast membrane lipid, leads to oxylipin overproduction and phloem cap lignification in *Arabidopsis*. *Plant Cell* 28: 219–232.

Linster, E. and Wirtz, M. (2018) N-terminal acetylation: an essential protein modification emerges as an important regulator of stress responses. *J. Exp. Bot.* 69: 4555–4568.

Lintala, M., Allahverdiyeva, Y., Kidron, H., Piippo, M., Battchikova, N., Suorsa, M., et al. (2007) Structural and functional characterization of ferredoxin-NADP+-oxidoreductase using knock-out mutants of *Arabidopsis*. *Plant J.* 49: 1041–1052.

Liszczak, G., Arnesen, T. and Marmorsteins, R. (2011) Structure of a ternary Naa50p (NAT5/SAN) N-terminal acetyltransferase complex reveals the

molecular basis for substrate-specific acetylation. *J. Biol. Chem.* 286: 37002–37010.

Li, D., Wei, J., Peng, Z., Ma, W., Yang, Q., Song, Z., et al. (2020) Daily rhythms of phytomelatonin signaling modulate diurnal stomatal closure via regulating reactive oxygen species dynamics in *Arabidopsis*. *J. Pineal Res.* 68: 1–12.

Li, H.M. and Yu, C.W. (2018) Chloroplast galactolipids: the link between photosynthesis, chloroplast shape, jasmonates, phosphate starvation and freezing tolerance. *Plant Cell Physiol.* 59: 1128–1134.

Ludwig-Müller, J. (2011) Auxin conjugates: their role for plant development and in the evolution of land plants. *J. Exp. Bot.* 62: 1757–1773.

Magin, R.S., March, Z.M. and Marmorstein, R. (2016) The N-terminal acetyltransferase Naa10/ARD1 does not acetylate lysine residues. *J. Biol. Chem.* 291: 5270–5277.

Müller-Moulé, P., Conklin, P.L. and Niyogi, K.K. (2002) Ascorbate deficiency can limit violaxanthin de-epoxidase activity in vivo. *Plant Physiol.* 128: 970–977.

Müller-Moulé, P., Golan, T. and Niyogi, K.K. (2004) Ascorbate-deficient mutants of *Arabidopsis* grow in high light despite chronic photooxidative stress. *Plant Physiol.* 134: 1163–1172.

Mulo, P., Sirpiö, S., Suorsa, M. and Aro, E.M. (2008) Auxiliary proteins involved in the assembly and sustenance of photosystem II. *Photosynth. Res.* 98: 489–501.

Nilsson, A.K., Fahlberg, P., Ellerström, M. and Andersson, M.X. (2012) Oxo-phytodienoic acid (OPDA) is formed on fatty acids esterified to galactolipids after tissue disruption in *Arabidopsis thaliana*. *FEBS Lett.* 586: 2483–2487.

O'Leary, B.M., Scafaro, A.P., Fenske, R., Duncan, O., Ströher, E., Petereit, J., et al. (2020) Rubisco lysine acetylation occurs at very low stoichiometry in mature Arabidopsis leaves: implications for regulation of enzyme function. *Biochem* 477: 3885–3896.

Olesova, D., Galba, J., Piestansky, J., Celusakova, H., Repiska, G., Babinska, K., et al. (2020) A novel UHPLC-MS method targeting urinary metabolomic markers for autism spectrum disorder. *Metabolites* 10: 1–12.

Porra, R.J., Thompson, W.A. and Kriedemann, P.E. (1989) Determination of accurate extinction coefficients and simultaneous equations for assaying chlorophylls *a* and *b* extracted with four different solvents: verification of the concentration of chlorophyll standards by atomic absorption spectroscopy. *Biochim. Biophys. Acta Bioenerg.* 975: 384–394.

Rantala, M., Paakkarinen, V. and Aro, E.M. (2018) Analysis of thylakoid membrane protein complexes by blue native gel electrophoresis. *J. Vis. Exp.* 139: 1–6.

Rantala, M., Ivanauskaite, A., Laihonen, L., Kanna, S.D., Ughy, B. and Mulo, P. (2022) Chloroplast acetyltransferase GNAT2 is involved in the organization and dynamics of thylakoid structure. *Plant Cell Physiol.* 63: 1205–1214.

Sainis, J.K., Dani, D.N. and Dey, G.K. (2003) Involvement of thylakoid membranes in supramolecular organisation of Calvin cycle enzymes in *Anacystis nidulans*. *J. Plant Physiol.* 160: 23–32.

Sampath, V., Liu, B., Tafrov, S., Srinivasan, M., Rieger, R., Chen, E.I., et al. (2013) Biochemical characterization of Hpa2 and Hpa3, two small closely related acetyltransferases from *Saccharomyces cerevisiae*. *J. Biol. Chem.* 288: 21506–21513.

Sasso, S., Dalmedico, L., Delwing-Dal Magro, D., Wyse, A.T.S. and Delwing-de Lima, D. (2014) Effect of N-acetylarginine, a metabolite accumulated in hyperargininemia, on parameters of oxidative stress in rats: protective role of vitamins and L-NAME. *Cell Biochem. Funct.* 32: 511–519.

Schreiber, U. and Klughammer, C. (2008) New accessory for the DUAL-PAM-100: The P515/535 module and examples of its application. *PAM Appl. Notes.*

Schaller, A. and Stintzi, A. (2009) Enzymes in jasmonate biosynthesis—structure, function, regulation. *Phytochemistry* 70: 1532–1538.

Schmidt, C., Beilsten-Edmands, V., Mohammed, S. and Robinson, C. (2017) Acetylation and phosphorylation control both local and global stability of the chloroplast F1 ATP synthase. *Sci. Rep.* 7: 1–11.

Scholz, S.S., Reichelt, M., Boland, W. and Mithöfer, A. (2015) Additional evidence against jasmonate-induced jasmonate induction hypothesis. *Plant Sci.* 239: 9–14.

Stintzi, A., Weber, H., Reymond, P., Browse, J. and Farmer, E.E. (2001) Plant defense in the absence of jasmonic acid: the role of cyclopentenones. *Proc. Natl. Acad. Sci. U.S.A.* 98: 12837–12842.

Sumner, L.W., Amberg, A., Barrett, D., Beale, M.H., Beger, R., Daykin, C.A., et al. (2007) Proposed minimum reporting standards for chemical analysis Chemical Analysis Working Group (CAWG) Metabolomics Standards Initiative (MSI). *Metabolomics* 3: 211–221.

Suss, K.-H., Arkona, C., Manteuffel, R. and Adler, K. (1993) Calvin cycle multienzyme complexes are bound to chloroplast thylakoid membranes of higher plants *in situ*. *Proc. Natl. Acad. Sci. U.S.A.* 90: 5514–5518.

Taki, N., Sasaki-Sekimoto, Y., Obayashi, T., Kikuta, A., Kobayashi, K., Ainai, T., et al. (2005) 12-oxo-phytodienoic acid triggers expression of a distinct set of genes and plays a role in wound-induced gene expression in *Arabidopsis*. *Plant Physiol.* 139: 1268–1283.

Tan, D.X. and Reiter, R.J. (2020) An evolutionary view of melatonin synthesis and metabolism related to its biological functions in plants. *J. Exp. Bot.* 71: 4677–4689.

Tsugawa, H., Cajka, T., Kind, T., Ma, Y., Higgins, B., Ikeda, K., et al. (2015) MS-DIAL: data-independent MS/MS deconvolution for comprehensive metabolome analysis. *Nat. Methods* 12: 523–526.

Ud-Din, A.I.M.S., Tikhomirova, A. and Roujeinikova, A. (2016) Structure and functional diversity of GCN5-related N-acetyltransferases (GNAT). *Int. J. Mol. Sci.* 17: 1018.

Uhrig, R.G., Schläpfer, P., Roschitzki, B., Hirsch-Hoffmann, M. and Gruissem, W. (2019) Diurnal changes in concerted plant protein phosphorylation and acetylation in *Arabidopsis* organs and seedlings. *Plant J.* 99: 176–194.

Verbruggen, N. and Hermans, C. (2008) Proline accumulation in plants: a review. *Amino Acids* 35: 753–759.

Wasternack, C. and Feussner, I. (2018) The oxylipin pathways: biochemistry and function. *Annu. Rev. Plant Biol.* 69: 363–386.

Weber, H., Vick, B.A. and Farmer, E.E. (1997) Dinor-oxo-phytodienoic acid: a new hexadecanoid signal in the jasmonate family. *Proc. Natl. Acad. Sci. U.S.A.* 94: 10473–10478.

Wu, X., Oh, M.H., Schwarz, E.M., Larue, C.T., Sivaguru, M., Imai, B.S., et al. (2011) Lysine acetylation is a widespread protein modification for diverse proteins in *Arabidopsis*. *Plant Physiol.* 155: 1769–1778.

Xue, C., Liu, S., Chen, C., Zhu, J., Yang, X., Zhou, Y., et al. (2018) Global proteome analysis links lysine acetylation to diverse functions in *Oryza sativa*. *Proteomics* 18: 1700036.

Yow, G.Y., Uo, T., Yoshimura, T. and Esaki, N. (2004) D-amino acid-N-acetyltransferase of *Saccharomyces cerevisiae*: a close homologue of histone acetyltransferase Hpa2p acting exclusively on free D-amino acids. *Arch. Microbiol.* 182: 396–403.

Yow, G.Y., Uo, T., Yoshimura, T. and Esaki, N. (2006) Physiological role of D-amino acid-N-acetyltransferase of Saccharomyces cerevisiae: Detoxification of D-amino acids. *Arch. Microbiol.* 185: 39–46.